Stellar Atlas

Project by Aniket Mishra

10/07/2025

Abstract

This document presents an independent project by Aniket Mishra, a BS-MS student at IISER Kolkata, aimed at simulating and analyzing the evolution of stars using theoretical models. The primary focus is on understanding stellar behavior through Hertzsprung–Russell (HR) diagrams by varying stellar mass and metallicity. Alongside HR diagrams, this study explores key evolutionary indicators such as core temperature versus core density (Tc vs ρc), age versus radius, age versus luminosity, and central hydrogen fraction versus time. These visualizations and analyses collectively provide insights into the internal structure, fusion processes, and life cycles of stars. A detailed explanation of the methodology, results, and interpretation is presented in the subsequent sections of this document.

Contents

Figures

Code listings

Chapter 1
Introduction

1.1 Background

Stellar evolution is the process by which stars evolve. This document is the project report of an independent study carried by Aniket Mishra, BS-MS student of IISER Kolkata. The project included studying the evolutionary course of a stars life and then studying the stars simulation ran using MESA(Modules for Experiments in Stellar Astrophysics)[1]. The project contains simulation data which is available on Zenodo[2] along with the necessary files required to run the simulations.

Stellar evolution, the process by which a star changes over the course of its life, is one of the most fundamental areas of study in astrophysics. Stars are not static entities; their physical structure, composition, and observable characteristics evolve dramatically due to internal nuclear fusion processes and energy transport mechanisms. Understanding how stars form, evolve, and ultimately die is essential to explaining the chemical enrichment of galaxies, the formation of exotic objects like neutron stars and black holes, and the broader dynamics of the cosmos.

Two of the most significant parameters that determine a star's evolutionary path are its initial mass and metallicity (the fraction of elements heavier than helium). Mass primarily controls the rate of nuclear burning and the star's luminosity, while metallicity influences opacities, fusion efficiency, and mass loss through stellar winds. These parameters together shape the lifetime, internal structure, and final fate of a star.

This project draws conceptual and theoretical guidance from *An Introduction to the Theory of Stellar Structure and Evolution* by Dina Prialnik[3], which provides the foundational physics governing stellar interiors and their time-dependent behavior.

1.2 Motivation

The motivation for this project stems from a desire to gain a deeper understanding of stellar evolution by directly simulating stars under a wide variety of physical conditions. While many textbooks and academic resources describe stellar behavior for typical solar-mass stars, comprehensive visual comparisons across a broad range of masses and metallicities are often absent or difficult to access. This project aims to bridge that gap by generating an "atlas" of evolutionary tracks, making it easier to visualize and interpret stellar changes as a function of these parameters.
Moreover, working independently on this simulation-based project allowed for a hands-on understanding of computational astrophysics using tools like MESA, reinforcing theoretical knowledge with direct experimentation and visualization.

1.3 Objectives

The primary objectives of this project are:

1. To simulate the evolutionary tracks of stars across a range of initial masses and metallicities using the MESA code.
2. To analyze and compare the resulting **Hertzsprung–Russell (HR) diagrams**, which reflect changes in stellar luminosity and surface temperature.
3. To generate and interpret additional plots such as:
    a. **Core temperature vs. core density (T_c vs ρ_c)**
    b. **Age vs. radius**
    c. **Age vs. luminosity**
    d. **Central hydrogen fraction vs. time**
4. To understand how **mass** and **metallicity** affect **nuclear fusion rates, stellar lifetimes, internal structures, and end states of stars.**
5. To document and present this work in an accessible and educational format that could serve as a reference for others studying stellar evolution.

1.4 Project Outline

The document is organized as follows:

- **Chapter 2: Theoretical Background -** Explains the necessary theory and equations in depth following the pattern of dina prialnik, also including certain theoretical topics for completeness, even if not directly related to simulation outputs.
- **Chapter 3: Methodology -** Describes the simulation setup, parameters chosen for mass and metallicity, and the software tools used (primarily MESA and Python).
- **Chapter 4: Results -** The simulation results are discussed here along with some important graphs included, on the scale of individual metallicities.
- **Chapter 5: Discussion -** This section compares trends across models, reflects on physical interpretations, and connects results to theoretical expectations.
- **Chapter 6: Conclusion -** Summarizes the key findings and suggests potential extensions of this work.
- **Appendices:** Includes relevant technical details, code snippets, and references.

Chapter 2
Theoretical Background

2.1 Introduction to stars

What defines a star?
At its most basic, a star can be defined by **two key characteristics**[3] :

1. It's a massive **collection of particles**, primarily gas, held together by its **own gravity**. Gravity is the force that attracts all objects toward one another, and in a star, it's what keeps all the gas from simply floating away.
2. It **radiates energy**, producing **light** and **heat** from internal sources. This energy is generated through nuclear fusion, a process we'll discuss later.

How is a star is formed?

The process of star formation starts with a large interstellar cloud consisting mostly of hydrogen and helium.
The gaseous cloud is often subjected to perturbations originating due to propagation of shock waves from a nearby supernova explosion, or due to collision with another chunk of cloud.
If at some region due to the perturbations, the density of gas increases, the gravitational pull is also increased. The gas pressure will also increase, but it will not necessarily be the amount required to maintain hydrostatic equilibrium(Chapter 2.2). The outcome of the perturbation depends on the dynamical stability of the region.
Using the *partial virial theorem* and an ideal gas *Equation Of State*, we get the stability condition as:

$$R \geq \frac{\alpha}{3}\frac{\mu G M}{K T}, \tag{2.1}$$

$$\begin{gathered}
\text{where R} = \text{Radius, K} = \text{ideal gas constant,} \\
\alpha = \text{a constant of order unity,} \mu = \frac{1}{\mu_{\mathrm{I}}} + \frac{1}{\mu_{\mathrm{e}}}, \\
\frac{1}{\mu_{\mathrm{e}}} = \text{average number of free electrons per nucleon,} \\
\frac{1}{\mu_{\mathrm{I}}} = \text{ mean atomic mass of stellar material,} \\
\text{G} = \text{Gravitational constant , M} = \text{Mass, T} = \text{Temperature}
\end{gathered} \tag{2.2}$$

The equality is obtained when the whole cloud is involved. A critical radius is hence defined at equality and the radius at equality is known as *Jeans radius(R_J)*. Hence, a upper limit for the mass may be obtained which may be contained in a volume at hydrostatic equilibrium, this mass is known as *Jeans mass*(M_J)

$$\begin{gathered}
M_{\mathrm{J}} = 10^5 \frac{T^{\frac{3}{2}}}{\sqrt{n}} M_{\odot}, \\
\text{where T is Temperature, } M_{\odot} \text{is sun's mass} \\
\text{and n is the number of gas particles per } m^3
\end{gathered} \tag{2.3}$$

A region within a gas cloud held together by its own gravity, with a mass comparable to that of a star, can be considered the nucleus of a future star. As it continues to grow by accreting surrounding material, the gravitational energy released during this process is converted into thermal energy. The increase in temperature and density raises the opacity of the gas. When the contracting gas becomes opaque to its own radiation, it enters the stage known as a **stellar embryo**. When hydrostatic equilibrium has been achieved, it is said to have become a **protostar**. *(prialnik, 2010)*
Till now no nuclear fusion has occurred within our newly developing star. As the core temperature rises and reaches around $\sim 10^7$K, the hydrogen fusion(hydrogen burning) starts, leading the **protostar** to become an **main sequence star**.

The stages of a star formation:

As discussed above, at the birth of a star hydrogen burning starts, providing enough energy and radiation to fulfill the second condition of the definition. The main stages of the star are:

1. **Main Sequence star:**
2. **Red Giant:**

3. Depending on the initial mass of the star, there are two different branches which could be derived after the red giant stage:
    a. **Planetary nebulae:**
        i. **White Dwarf:**
    b. **Supernovae:**
        i. **Neutron star:**

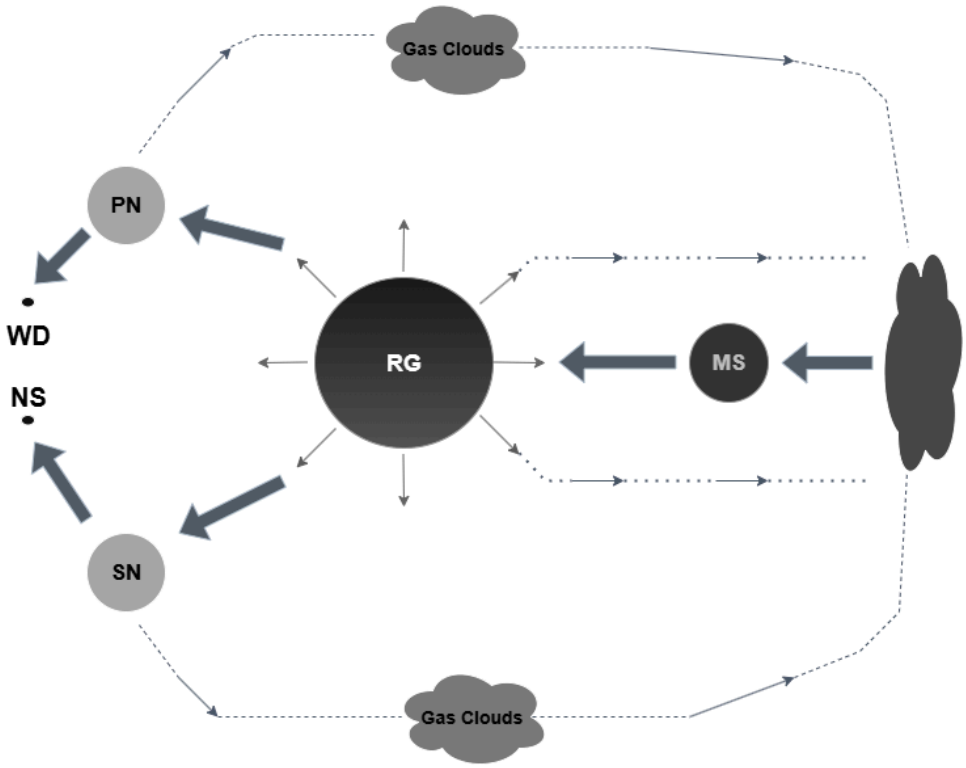

Figure 2.1: A schematic representation of stellar evolution. Stars form from gas clouds, evolve through the main sequence (MS) and red giant (RG) phases. Low-mass stars become planetary nebulae (PN) and white dwarfs (WD); high-mass stars explode as supernovae (SN), leaving neutron stars (NS). The cycle continues as expelled material forms new stars.

2.2 Necessary Equations

This section was adapted and heavily inspired from “An introduction to stellar evolution” by Dinal Prialnik[3] and hence there may be some unconscious overlap between the two from my side.

1. **The Balancing Act: Hydrostatic Equilibrium:** Imagine a tiny particle somewhere deep inside a star. This particle experiences two opposing forces:
   - **Gravity:** Pulling it inward, towards the star's core.
   - **Pressure:** Pushing it outward, away from the core.

   Hydrostatic equilibrium is the state where these two forces are perfectly balanced at a given radius within the star. The equation derived for this condition is :

$$\frac{dP}{dr} = -\frac{\rho G m}{r^2} \tag{2.4}$$

   or

$$\frac{dP}{dm} = -\frac{Gm}{4\pi r^4}$$

   where $\frac{dP}{dr}$ is the change in pressure with respect to radius, ρ is the density of the stellar material, G is the gravitational constant, m is the mass enclosed within radius r, r is the radial distance from the center of the star.
   This equation tells us that the pressure inside a star must increase as you move closer to the core to counteract the increasing gravitational force.

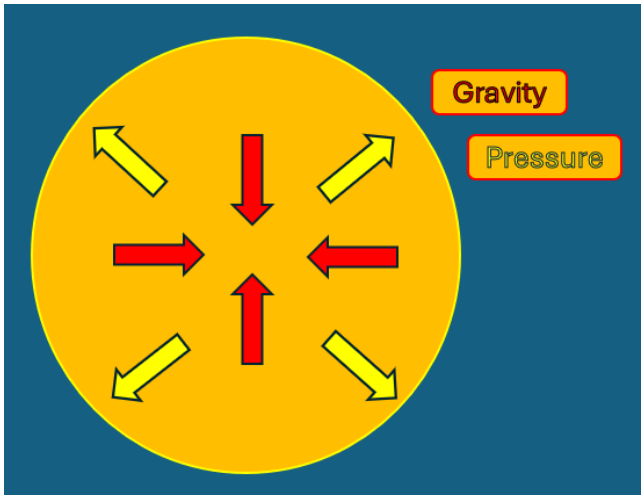

   Figure 2.2: Hydrostatic equilibrium is achieved when the inward gravitational force is exactly balanced by the outward pressure at each point inside the star.

2. **The equation of Energy:** So, where does a star get its energy? The answer lies in nuclear fusion, a process that occurs in the star's core. At the immense temperatures and pressures found there, hydrogen atoms are forced together to form helium, releasing a tremendous amount

of energy in the process. This process can be explained by the famous equation E=mc², where a small amount of mass is converted into a large amount of energy. This energy is what makes stars shine. We use the first law of thermodynamics which says that the internal energy may change by two forms of energy transfer: Heat and work. We derive the following equation with this:

$$\dot{u} + P\left(\frac{\dot{1}}{\rho}\right) = q - \frac{\partial F}{\partial m} \tag{2.5}$$

where we used $\dot{f}$ notation for the temporal derivative $\frac{\partial f}{\partial t}$, u is internal energy per unit mass, and q is the rate of nuclear energy release per unit mass

3. **Spherical Symmetry:** In the majority of the cases, the stars are symmetrical in shape, because gravity is a spherically symmetric force, that is, gravity is same radially (at the same radius 'r', the gravity is same). Hence ,we neglect the cases deviating from spherical symmetry. Assuming the star to be a sphere, we get a relation between mass, density and radius as:

$$\frac{dm}{dr} = 4\pi r^2 \rho \tag{2.6}$$

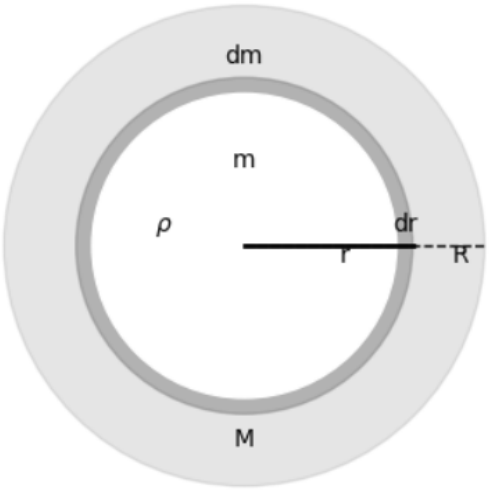

Figure 2.3: A figure showing spherical symmetry of the star and thereby the various quantities which gives relationship between r and m.

4. **The equations governing the composition changes:** The material inside a star is composed of free electrons and atomic nuclei. Due to the extreme conditions, chemical reactions are impossible; only nuclear reactions can occur, changing one nucleus into another.
   To understand this further, we need basic knowledge about the nucleus:
   - Atomic nuclei is made up of protons and neutrons, collectively called nucleons and they belong to the group of heavy particles called baryons. The particles are characterized by two numbers, A (Baryon number) and Z (charge); for proton (1,+1) and for neutron (1,0).
   - Electrons and neutrinos are leptons—light particles with zero baryon number. Neutrinos have no charge and accompany leptons in nuclear processes to conserve quantum numbers.
   - Two types of forces act in the nucleus, strong nuclear force, the force of attraction which binds the nucleus together and the weak interaction force, which is responsible for changing protons into neutrons and vice-versa.
   - In nuclear reactions, charge, baryon number, and lepton number are always conserved. For example, weak interactions involve electrons or positrons to balance charge, and neutrinos or antineutrinos to conserve lepton number.

   As a nucleus of any element is uniquely defined by two integers, A and Z, a nuclear reaction might look like:

   $$I(A_i, Z_i) + J(A_j, Z_j) \leftrightarrows K(A_k, Z_k) + L(A_l, Z_l)$$

   which is subject to two conservation laws:
   - $A_i + A_j = A_k + A_l$
   - $Z_i + Z_j = Z_k + Z_l$

   After some derivations, we can derive the following equation for the rate of change of mass fraction:

   $$\frac{\dot{X}_i}{A_i} = \frac{\rho}{m_h}\left(-\frac{X_i}{A_i}\sum(1+\delta_{ij})\frac{X_j}{A_j}\frac{R_{ijk}}{1+\delta_{ij}} + \sum\frac{X_l}{A_l}\frac{X_k}{A_k}\frac{R_{lki}}{1+\delta_{lk}}\right) \quad (2.7)$$

   where, X_i is the mass fraction of species i, A_i is the atomic mass number of species i, ρ is the density, m_h is the mass of a hydrogen atom, R_{ijk} is the rate of the nuclear reaction involving species i, j, and k, δ_{ij} is the Kronecker delta (1 if i=j, 0 otherwise).
   For simplicity we will define a composition vector by $X \equiv (X_1, \ldots, X_n)$ so that the set of equations from 1 to n may be collectively written as: $\dot{X} = \mathbf{f}(\rho, T, X)$

When the rate of change of mass fraction is zero ($\dot{X} = 0$), the star is in nuclear equilibrium.

2.3 Polytropic models

In the study of stellar structure, obtaining exact analytical solutions to the full set of equations talked about before is rarely feasible due to their non-linear and coupled nature. To make the problem more tractable, simplifying assumptions are often introduced. One such approach is the polytropic model, which assumes a specific relationship between pressure(P) and density(ρ) of the form:

$$P = K\rho^{\gamma} \tag{2.8}$$

where K and γ are constants. This is known as the polytropic equation of state (EOS). The exponent γ is related to the polytropic index n by the relation,
$\gamma = 1 + \frac{1}{n}$
A notable physical system that follows a polytropic equation of state is a completely degenerate electron gas. In this case, the polytropic index n takes a value of 1.5 in the non-relativistic limit, and 3 in the relativistic limit, depending on the pressure-density relationship dictated by quantum statistics. To determine the structure of a star following this model, we substitute the equation of state in the 4 equations of the previous section to get a second-order differential equation known as **Lane-Emden equation:**

$$\frac{1}{\xi^2}\frac{d}{d\xi}\left(\xi^2\frac{d\theta}{d\xi}\right) = -\theta^n \tag{2.9}$$

where, ξ is a dimensionless variable relating to radius, θ is radial variable determining how density changes with radius, n is the polytropic index. The equation is subject to boundary condition $\theta(0) = 1$ and $\theta'(0) = 0$ corresponding to a normalized central density and a regular center. Numerical solution of this equation provides the density and pressure profiles of stars modelled as polytropes. While simplified, the Lane–Emden equation remains insightful for modeling stellar structure, particularly in systems like white dwarfs.
For further details, including mass-radius relations and the significance of different n values, the reader is referred to Prialnik (2009).
While the polytropic models do not provide exact solutions and break down under certain conditions, they still provide a good enough solution to otherwise intractable equations and allow useful scaling laws for mass, radius, and central pressure.

2.4 Nuclear processes in stars

To understand the nuclear processes going on in a star, we first need to understand the concept of binding energy

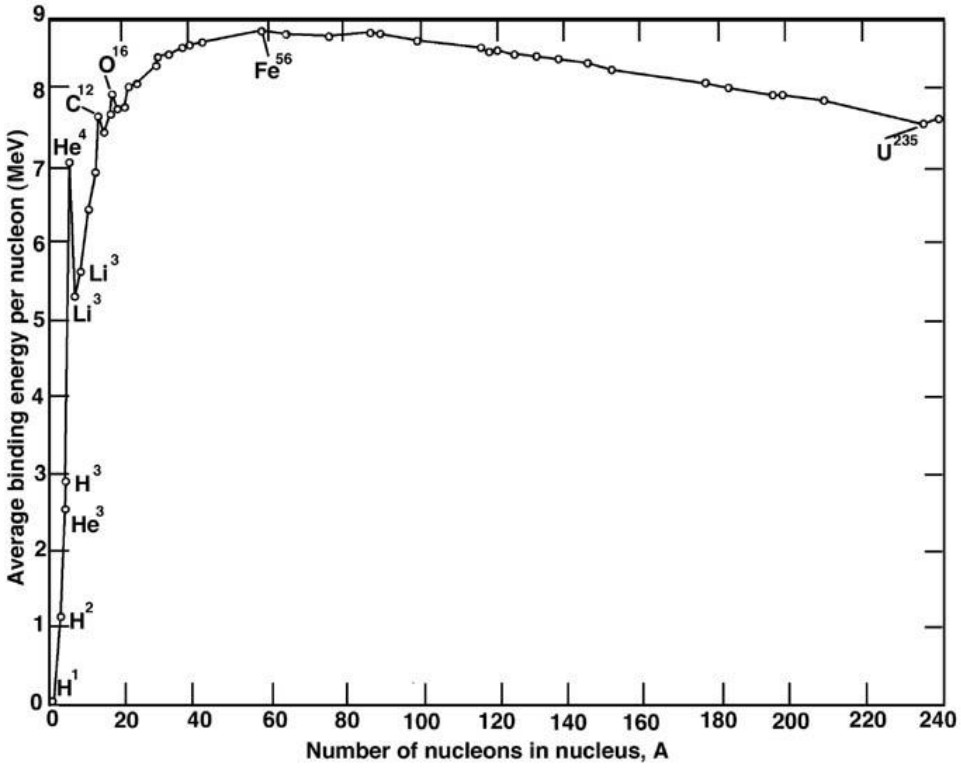

Figure 2.4: Average binding energy per nucleon as a function of nucleon number. The peak near iron-56 indicates maximum nuclear stability, illustrating why fusion of lighter elements up to Fe releases energy and why fission of heavier elements likewise releases energy. **Image credit: Wikimedia Commons (public domain).**

As seen in Figure 2.4, the binding energy per nucleon increases from hydrogen up to iron-56, indicating that fusion of light nuclei into heavier ones releases energy. Beyond iron, the curve declines, meaning that fission of heavier elements also releases energy. This explains why fusion powers stars and why fission powers nuclear reactors.
Stars are primarily composed of hydrogen and helium, with heavier elements (“metals”) making up only about 0.001–4% of the total mass. Consequently, hydrogen is the first element to undergo fusion in stellar interiors.

1. **Hydrogen Burning:** Occurs in the stellar core via two processes: the proton–proton (p–p) chain in low-mass stars and the CNO bi-cycle in higher-mass stars.
2. **Helium Burning:** Once hydrogen is exhausted, helium fuses into carbon via the triple-α process.
3. **Carbon-Oxygen burning:** These elements, formed from helium burning, ignite at higher temperatures in more massive stars.
4. **Si burning:** At very high core temperatures, silicon fuses into iron-group elements such as Fe, Co, and Ni.

The synthesis of iron marks the end of exothermic nuclear burning in a star, as further fusion becomes energetically unfavorable. This series of fusion reactions is collectively known as stellar nucleosynthesis. At extreme temperatures during core collapse, photodisintegration can occur—where high-energy gamma photons break iron nuclei into alpha particles and free neutrons, effectively reversing nucleosynthesis and triggering runaway collapse.

2.5 The star's mass loss

Mass loss is a key factor in the evolution of many stars, particularly high-mass and red giant stars. It occurs through stellar winds driven by radiation pressure, surface pulsations, and convection. In hot, luminous stars, radiation on metal lines leads to significant outflows, while in cooler giants, dust and molecular opacity enhance wind efficiency. These processes gradually strip the outer envelope, shortening the star's life, altering its evolutionary track, and determining the final remnant mass.
Although MESA supports mass loss modeling, the current simulations do not include any mass-loss prescriptions. This choice simplifies the model space but may lead to overestimates of final core mass and deviations from realistic post-main-sequence behavior in massive stars.

2.6 The evolution of stars

A newly formed star is considered homogenous with hydrogen and helium mixed together. As the nuclear burning begins, and the star evolves, it develops a layered structure driven by fusion and convection.

- In the main-sequence stars, the hydrogen is burned in the core, while in the outer layer no nuclear exothermic reaction happens. Radiative and Convective zones may thus form depending on the star's mass.

- In the post-main sequence, a hydrogen burning shell is formed around the core which is now burning helium. The helium burning in the core creates Carbon/Oxygen and the hydrogen shell burning produces helium. Hence, due to these processes, an "onion-like" structure is formed in the star's interior.

Thermodynamic gradients: Alongside compositional changes, stellar interiors become more stratified in temperature and density. In high-mass stars, this leads to radiation-dominated cores and advanced fusion stages; in low-mass stars, it leads to degeneracy and eventual white dwarf formation.

Implication for this project: These internal changes are indirectly reflected in the simulated tracks, particularly in temperature–density evolution, core mass growth, and HR diagram loops. Later sections visualize these transitions across mass ranges.

2.7 Understanding HR diagrams

The HR diagram stands for Hertzsprung-Russel diagram, named after two astronomers, Ejnar Hetzsprung and Henry Norris Russel. Temperature and Luminosity are the two most fundamental properties of stars which can be deduced by just observation, hence the diagram whose axes are Temperature or its related properties and Luminosity or its related property is known as HR diagram.

The horizontal axis generally represents the surface temperature of the star, usually plotted as $\log(T_{eff})$ (in kelvin). Also, Conventionally, it is inverted with the value increasing from right to left. The vertical axis represents Luminosity, either in absolute units ($\log(L/L_{\odot})$) or absolute magnitude (in observational plots) which tells us how bright a star is when compared to the Sun.

When the diagram is plotted, one may notice that most of the stars lie along a diagonal line, which raises the question: are there any areas on the diagram stars can't exist on? This is very beautifully explained in prialnik(2010), which describes the physical limits of stellar stability and structure. The stars lying on the prominent diagonal band are known as main-sequence stars. The position of a star on the HR diagram is determined by its initial mass:

1. High-mass stars are hot and luminous → appear at the top-left
2. Low-mass stars are cool and dim → appear at the bottom-right

As stars deplete the hydrogen in their core, they evolve off the main sequence, entering the new regions of the diagram.

- Red Giants: Cooler but more luminous, formed as low- to intermediate-mass stars expand

- White Dwarfs: Hot but faint (remnants of low-mass stars that shed their outer layers)
- Supergiants: Evolved stages of high-mass stars, highly luminous but relatively cool

The HR diagram is more than just a scatter plot, it is a map of stellar life cycles. A single star moves along a path (called an evolutionary track) through the diagram as it evolves:

- Enters at the Zero-Age Main Sequence (ZAMS)
- Moves towards high luminosity as fusion shifts to shell burning
- Eventually contracts or explodes, depending on the mass.

The HR diagram, therefore, serves as both a snapshot of stellar populations and a dynamic framework for understanding how stars change with time. It is indispensable in both theoretical astrophysics and observational astronomy.

2.8 The Stellar Life Cycle

With this section, we conclude the theoretical groundwork of stellar structure and evolution, equipping the reader with the tools to interpret the rest of this project.

Stars are dynamic objects, constantly changing throughout their lives. The forces that drive their evolution include:

- Gravity
- Pressure (thermal and degeneracy)
- Nuclear energy generation
- Radiation and opacity

In earlier sections, we examined how these forces are balanced and quantified through fundamental equations. These form the basis for modeling and simulating the internal structure and long-term behavior of stars.

Among all stellar properties, the most decisive factor in a star's evolution is its *initial mass*. This single parameter determines a star's:

- Lifespan
- Luminosity
- Position on the HR diagram
- Nuclear burning phases
- Ultimate fate (white dwarf, neutron star, or black hole)

While this chapter developed a theoretical understanding of the stellar life cycle, we now turn to the computational side, using MESA to simulate stars. These models will not only help us visualize the theoretical pathways, but will also be compared to real observational data to test their validity.

The next chapter outlines the methods used to run these simulations and extract the physical quantities required for further analysis.

Chapter 3
Methodology

In this section, I will discuss the methodology I used to conduct this project.

3.1 Introduction to MESA

MESA[1], [4] (Modules for Experiments in Stellar Astrophysics) is a **1D stellar evolution code** that allows researchers to **simulate the structure** and **evolution of stars** across a wide range of masses and stages. It is written in **modern Fortran** and released under the **GNU General Public License v3.0**, making it freely available for educational and scientific use.

MESA's modular design enables great flexibility in customizing simulations, though this also means that the learning curve can be steep for first-time users. Its core components include:

1. **Main simulation module – `star` :** The primary driver of stellar evolution. It calls other internal physics modules as needed during a simulation.
2. **Equation of State (EOS):** Determines the thermodynamic properties of stellar matter. MESA includes a range of EOS options suitable for different temperature and density regimes.
3. **Opacity module:** Calculates radiative opacity based on temperature, density, and chemical composition. Type I and Type II opacity tables can be used depending on whether composition changes during evolution are considered.
4. **Nuclear Reaction Networks:** Define which nuclear processes (e.g., pp-chain, CNO cycle, triple-α) are active. Users can choose from a set of pre-defined networks or customize their own.

When used to its full potential, MESA offers an exceptionally powerful platform for modeling stellar evolution with high physical realism and repro-

ducibility. Its **open-source nature** and **active community** make it both robust and well-supported.

3.2 FFMPEG

FFmpeg[5] is a powerful **command-line utility** used for **processing** and **converting multimedia files**. It can be used to combine a sequence of images into a video, extract frames from a video, or convert between various formats.

In this project, **FFmpeg** was used to **stitch together** `.png` **image frames** generated by MESA during simulation runs. These frames, which show diagrams such as the HR diagram and temperature-density evolution, were compiled into continuous video sequences to visualize how a star evolves over time. This made it easier to interpret gradual changes in stellar properties during different phases of evolution.

3.3 Plotting using matplotlib

To visualize and analyze the raw simulation data produced by MESA, I used the Python library `matplotlib` [6] in combination with `mesa_reader` [7], a dedicated tool for **reading MESA output files** such as `history.data` and `profileN.data`.

These tools allowed me to generate plots like:

- Hertzsprung–Russell (HR) diagrams
- Central temperature vs central density
- Luminosity and radius over time
- Central hydrogen abundance as a function of age

The plots were customized using log scales, axis annotations, and line color coding to clearly reflect stellar evolution trends across different masses. This visual analysis formed the basis of the Stellar Atlas and enabled effective comparison between models.

3.4 Automating Simulations Using Bash Scripting

Since this project involved running a large number of stellar evolution simulations across different **initial masses**, executing each run **manually** would have been **inefficient** and **error-prone**. To address this, I used **Bash scripting** to **automate** the workflow.

Bash scripting allows users to write a sequence of terminal commands into a script file, which can then be executed line by line in the Bash shell. This made it possible to:

- **Generate folders for each simulation**
- **Copy and modify input files**
- **Launch MESA runs**
- **Automatically call post-processing scripts like** `rn.py`

The script use for the automation is available in **Appendix B**, the reader may refer to it. Automation ensured consistency across all simulations, eliminated repetition, and highlighted the reusability and scalability of the workflow.

3.5 Simulation Setup

With the overall workflow in place, the next step was to define the simulation parameters and configure the model space for this project.

The first parameter to decide was the **mass range** and **metallicity**. For the initial round of simulations, I selected a metallicity value of **0.02**, which corresponds to **solar metallicity**[1]. The stellar masses ranged from $\mathbf{0.5\,M_\odot}$ to $\mathbf{100\,M_\odot}$ in steps of $\mathbf{0.5\,M_\odot}$, leading to a dense sampling of the main sequence and post-main-sequence phases. Upon inspecting the results, I extended the **upper mass range** with additional values: **200, 350, 600, 800, and 900** $\mathbf{M_\odot}$, out of curiosity about how extremely massive stars evolve.

For a **single metallicity**, this resulted in **approximately 205 simulations**. These simulations typically took around **12 hours** to complete on my system. To explore how stellar evolution varies with metallicity, I extended this framework to include five additional metallicity values: **0.0001, 0.001, 0.006, 0.014, and 0.04** — each with the same mass distribution, bringing the total **simulation count per stopping condition** to **1230**.

Two stopping conditions were employed:

- **Hydrogen depletion**: When central hydrogen mass fraction fell below $\mathbf{10^{-5}}$
- **Helium depletion**: When central helium was exhausted i.e. when its mass fraction fell below $\mathbf{10^{-5}}$

In all cases, a secondary condition was imposed: simulations terminated if the model number exceeded 10,000. Hydrogen-depletion simulations focused

[1] While **older** stellar evolution models often used $\mathbf{Z = 0.02}$ as a proxy for **solar metallicity**, more recent solar abundance measurements suggest a lower value of $\mathbf{Z \sim 0.014}$ (e.g., **Asplund et al., 2009**[8]). For consistency with standard MESA setups and to maintain compatibility with available opacity tables, this project considers both values in the simulation set.

on analyzing the main-sequence phase, while helium-depletion simulations provided insights into red giant and post-main-sequence behavior. Mass loss was included in the helium-depletion runs but omitted from hydrogen-depletion simulations, which is physically acceptable since mass loss is generally negligible during the main sequence.

3.5.1 Workflow Summary

The complete simulation pipeline consisted of the following stages[2]:

1. **Inlist Generation**: A `.csv` file was created listing mass, metallicity, and stopping condition for each simulation. A Python script then read this data and filled out an `inlist` template accordingly, producing fully customized `inlist` files. This approach allowed rapid generation of hundreds of input configurations without manual repetition.
2. **Simulation Execution (via Bash)**: A Bash script handled automation at scale. For each model, it created a MESA working directory, inserted the correct `inlist`, and initiated the simulation. Upon completion, a Python script (`rn.py`) was executed to generate plots from the simulation output. Finally, FFmpeg compiled these plot frames into video animations, producing visual HR diagrams and central temperature-density evolution.

All code scripts and their logic are described in detail in the appendix.

3.6 Outputs (Data Analysis)

Given the large scale of simulations, analyzing the resulting plots, diagrams, and animations efficiently required a structured interface. To address this, I integrated all simulation outputs into a custom-built website developed using **Streamlit**, a Python-based framework for creating interactive web applications.

The website is organized by metallicity, with separate pages dedicated to each Z value. Within each page, simulations are sorted by stellar mass, allowing for intuitive navigation and comparison across the full parameter space. Each simulation entry displays:

- Key plots such as the HR diagram, central temperature vs central density, and age-luminosity curve

[2]Plots were generated using **matplotlib** and **mesa_reader**. **FFmpeg** was used to convert sequential **PNG outputs** from **MESA** into **video animations**. **Streamlit** was used to organize the results on a website. **Bash scripting** and **Python automation** were used extensively throughout the project. [5], [6], [7], [9]

- Automatically generated metadata including initial mass, metallicity, and stopping condition
- Short video animations created from frame sequences using FFmpeg

The visualizations were rendered using `matplotlib`, and metadata was extracted and formatted using a Python script into `.json` files during batch post-processing. A drop-down interface enables efficient browsing and side-by-side inspection of models.

This website serves as both a companion to this report and a reusable visual reference for future students and researchers exploring stellar evolution.

Chapter 4
Results

This chapter presents the results of the MESA simulations across a range of stellar masses and metallicities. The simulations were analyzed under two separate stopping conditions: core hydrogen depletion and core helium depletion. For each metallicity group, trends in stellar evolution are examined using the Hertzsprung–Russell (HR) diagram, age vs luminosity, age vs radius, central hydrogen abundance vs time, and central temperature vs density plots. This chapter does not explain the underlying physics in detail, but instead focusses on interpreting the outcomes of the simulation.

4.1 Stopping Condition - (Hydrogen < 1d-5):

In this section, we analyze and interpret the simulation result of each individual metallicity and than discuss the all over trend in this section.

4.1.1 Metallicity (Z) = 0.0001:

A metallicity of Z = 0.0001 corresponds to extremely metal-poor stars, with only 0.01% of their mass in elements heavier than helium. Such stars are known as Population III stars which are believed to be among the earliest formed in the universe. These stars are extremely rare or possibly no longer observable, making them astrophysically intriguing as simulation targets.

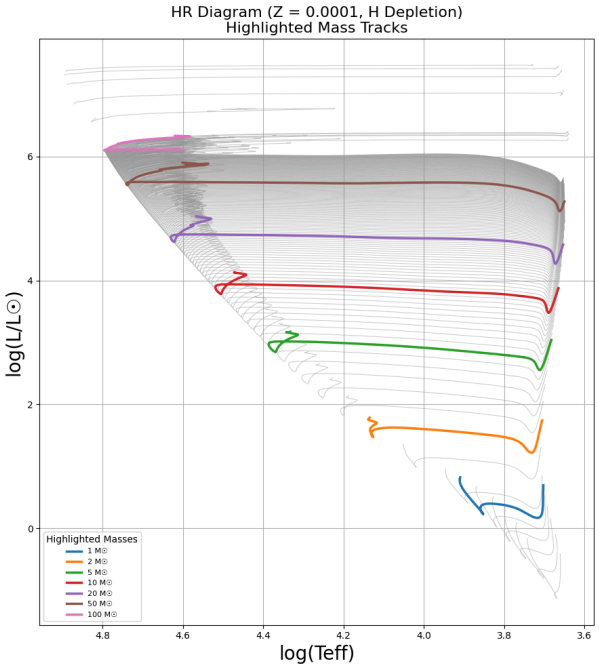

Figure 4.5: Hertzsprung-Russell diagram for stars with Z = 0.0001, evolved until core hydrogen is depleted. Tracks for selected masses (1, 2, 5, 10, 20, 50, 100 $M_\odot$) are highlighted, showing the dependence of stellar evolution on initial mass.

From the HR diagram, we can observe that as stellar mass increases, both the Surface temperature and luminosity also increase, which is to be expected following the stellar model. Since the stopping condition is core hydrogen exhaustion, only the main-sequence portion of evolution is captured.

The visibility of evolutionary loops decreases with increasing stellar mass, which is expected since higher-mass stars evolve more rapidly than their low-mass counterparts. This trend is evident in the HR diagram, where loops become faint or nearly vanish beyond 20 $M_\odot$. In contrast, lower-mass stars exhibit a more pronounced hook-like feature, marking the onset of core hydrogen exhaustion. Higher-mass stars evolving more rapidly than the low-mass ones can be cross-verified using the central hydrogen versus age plots available on the website or in the dataset.

The 100 $M_\odot$ track deviates from the expected pattern, likely due to numerical limitations, convergence issues, or the physical instability of such massive stars at extremely low metallicity.

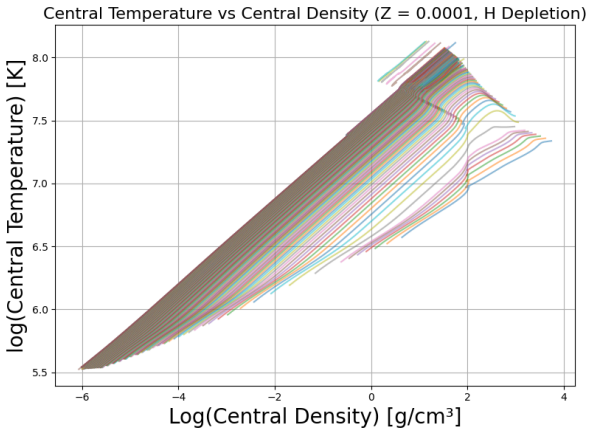

Figure 4.6: Evolution of central temperature versus central density for stars with Z = 0.0001 during the hydrogen-burning phase. Lower-mass stars curve toward the degeneracy regime, while higher-mass stars maintain thermally supported cores.

The central temperature vs. central density plot provides insights into the internal thermodynamic evolution of stars during hydrogen burning. In this diagram, lower-mass stars ($\sim$0.7 $M_\odot$) are seen curving toward the degenerate regime, they reach high central densities without corresponding increases in temperature, suggesting their cores are supported primarily by electron degeneracy pressure. This is consistent with their evolutionary path toward becoming white dwarfs.

For intermediate masses ($\sim 3\,M_\odot$), the tracks begin to bend in the direction of the degenerate branch but do not fully enter it. This indicates they are approaching degeneracy and may eventually reach it in later evolutionary stages if the simulation continued beyond hydrogen exhaustion.

Higher-mass stars evolve at higher temperatures and lower central densities due to stronger thermal pressure support. Their tracks remain on the thermally supported side of the diagram throughout this phase, consistent with expectations from stellar structure theory. Unlike low-mass stars, they do not become degenerate during the main sequence and are more likely to undergo advanced nuclear burning in later stages.

4.1.2 Metallicity (Z) = 0.001:

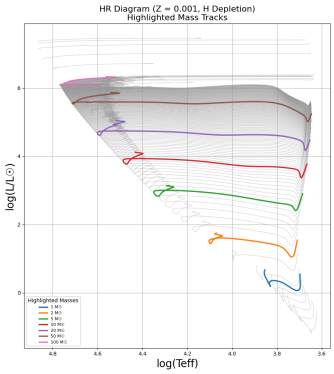

Figure 4.7: HR diagram for Z = 0.001 stars. Selected masses highlighted.

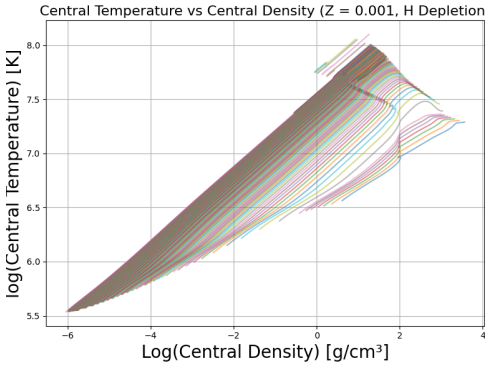

Figure 4.8: Central temperature vs. density for Z = 0.001 stars.

Compared to Z = 0.0001, the HR diagram for Z = 0.001 shows slightly broader tracks at lower masses, with reduced effective temperatures for similar mass stars. This reflects increased opacity from the higher metal content. However, the overall morphology remains similar, and no major shift in evolutionary patterns is observed within the mass range simulated. The central temperature vs. density tracks show a marginal reduction in maximum Tc for low- and mid-mass stars, consistent with enhanced radiative trapping at higher Z. The degeneracy onset behavior remains broadly unchanged.

4.1.3 Metallicity (Z) = 0.006:

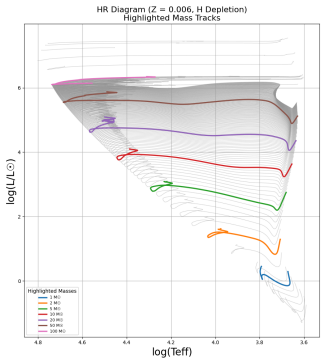

Figure 4.9: HR diagram for Z = 0.006 stars. Selected masses highlighted.

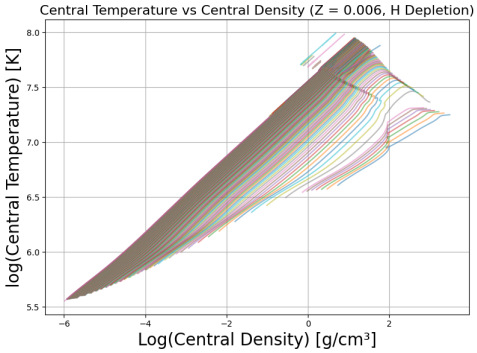

Figure 4.10: Central temperature vs. density for Z = 0.006 stars.

The trends seen in Z = 0.001 continue here, becoming more pronounced. The HR diagram shows even broader tracks at lower masses, and a further reduction in surface temperatures. In the Tc–ρc plot, central temperatures for low- and mid-mass stars continue to decline, dropping below log(Tc) = 8.0. This further confirms the role of metallicity in reducing core temperatures and enhancing energy trapping.

4.1.4 Metallicity (Z) = 0.014:

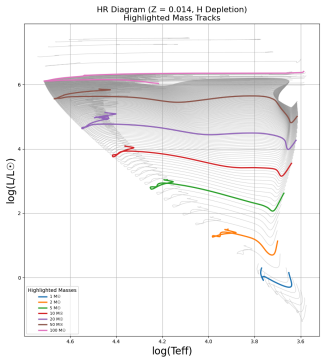

Figure 4.11: HR diagram at Z = 0.014 (highlighted tracks).

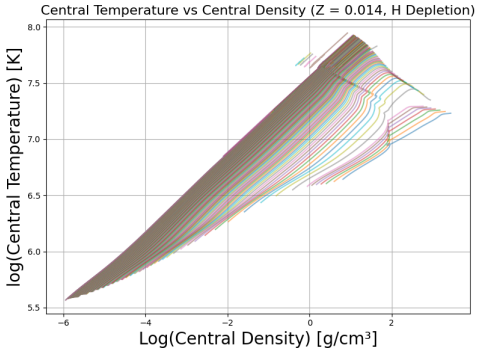

Figure 4.12: Tc vs. ρc for Z = 0.014 stars.

Z = 0.014 represents the commonly accepted modern solar metallicity. At this value, the HR diagram shows broadening of the lower-mass tracks continuing the trend seen in Z = 0.006. The hook features in low-mass stars remain visible, though slightly more compressed. Central temperature maxima decline further for stars below 10 $M_{\odot}$, consistent with metallicity-driven opacity effects reaching a plateau.

4.1.5 Metallicity (Z) = 0.02:

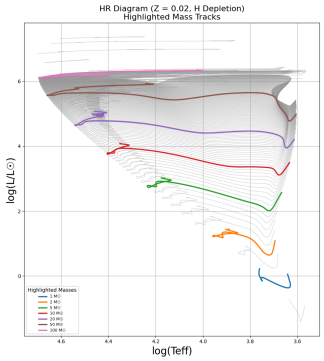

Figure 4.13: HR diagram at Z = 0.02 (highlighted tracks).

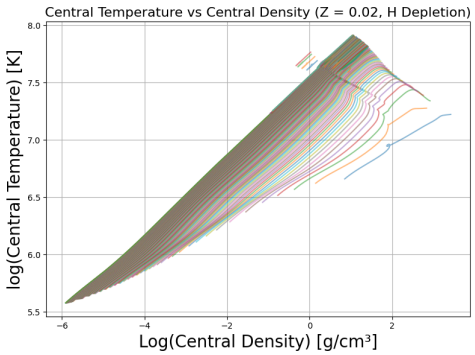

Figure 4.14: Tc vs. ρc for Z = 0.02 stars.

Z = 0.02 stars show marginally more extended tracks in the HR diagram for low- and mid-mass stars.

The evolutionary time scales for these stars are slightly longer, particularly for stars below 2 $M_{\odot}$.

Central density increases slightly at hydrogen exhaustion for low-mass stars compared to Z = 0.014.

This metallicity is the most stable for running simulations and hence is used widely in many studies and researches.

4.1.6 Metallicity (Z) = 0.04:

Z = 0.04 corresponds to an unusually metal-rich composition, which is rarely encountered in nature. From a simulation standpoint, this metallicity exhibits notable instability beyond masses of 60 $M_{\odot}$. In my runs, most stars above this threshold either failed during bulk simulations or produced incomplete results when run individually. This likely arises due to increased opacity and radiation pressure at high metallicity, making the stellar structure more sensitive and numerically unstable. Incorporating additional physical effects may be necessary to stabilize these stars, but such extensions are beyond the scope of this project. As a result, only simulations up to 60 $M_{\odot}$ are presented for Z = 0.04, unlike other metallicity sets that extend to much higher masses.

4.2 Stopping Condition - (Helium < 1d-5):

4.2.1 Metallicity (Z) = 0.0001:

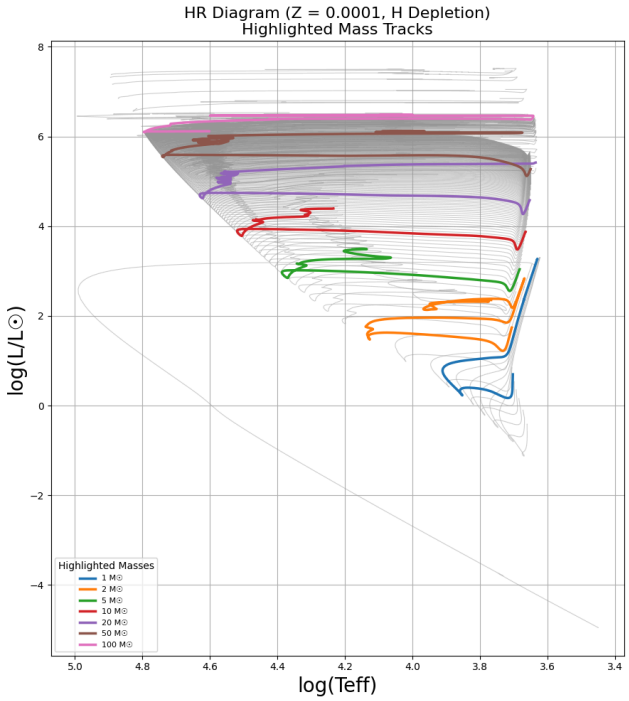

Figure 4.15: Hertzsprung-Russell diagram for stars with Z = 0.0001, evolved until core helium is depleted. Tracks for selected masses (1, 2, 5, 10, 20, 50, 100 $M_\odot$) are highlighted, showing the dependence of stellar evolution on initial mass.

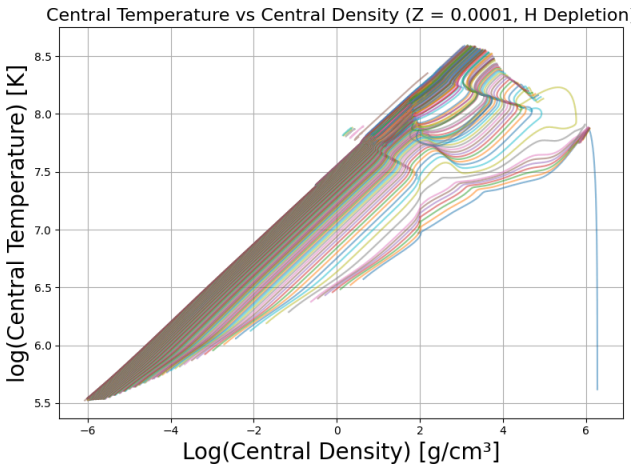

Figure 4.16:

4.2.2 Metallicity (Z) = 0.001:

4.2.3 Metallicity (Z) = 0.006:

4.2.4 Metallicity (Z) = 0.014:

4.2.5 Metallicity (Z) = 0.02:

4.2.6 Metallicity (Z) = 0.04:

4.3 Comparison with real data (GAIA3)

Having compared the simulations across different metallicities, we now turn to validating the results against observational data. For this purpose, we utilize the Gaia DR3 dataset to construct an observational Hertzsprung-Russell diagram. On the simulation side, we use the models evolved up to core helium exhaustion for Z = 0.02, which approximates solar metallicity. Both the simulated and observed HR diagrams will be overlaid on a single plot to allow direct comparison. All codes used to query, process, and plot the Gaia data are provided in the Appendix.

Chapter 5
Discussion

This project aimed to explore the theoretical and computational aspects of stellar evolution by simulating stars across a wide range of initial masses and metallicities using MESA. The results successfully reproduced the expected physical behavior of stars during the hydrogen-burning phase. In this chapter, we reflect on the trends observed, compare them to established theory and Gaia data, and assess the strengths and limitations of the simulation approach.

Based on the simulation results, the evolution of star is primarily governed by its initial mass and composition. High mass stars occupy the **top-left region** in the HR diagram and evolve rapidly due to higher core temperature and pressure. In contrast, low mass stars evolve more gradually and occupy the **lower-right region** of the diagram, with some entering degeneracy as hydrogen is depleted. Stars below $\sim \mathbf{0.7 M_\odot}$ show signs of degeneracy around hydrogen exhaustion, meaning that they are unlikely to evolve into a red giant phase and will follow a different path. These results closely follow classical models presented in Prialnik[3], especially the relationship between **core properties** and **evolutionary stage**.

Metallicity plays a **secondary** but **significant** role. As metallicity **increases**, the **opacity** within the stellar interior **rises**, leading to **reduced effective temperatures** and **broader HR tracks**. These trends are consistent with theoretical expectations and are most pronounced for low- to intermediate-mass stars. Interestingly, the trend begins to **saturate** beyond $\mathbf{Z = 0.014}$, with $\mathbf{Z = 0.02}$ and $\mathbf{Z = 0.04}$ showing only minor morphological differences. This plateau suggests that metallicity effects are most pronounced at sub-solar values.

The plots of **central temperature** versus **central density** further reinforce these trends. Low-mass stars **curve** toward **degeneracy** as **hydrogen is depleted**, while **higher-mass stars** maintain **thermally supported cores**. These trajectories help distinguish which stars are likely to evolve into **white dwarfs** and which will continue **fusion beyond helium**. The degeneracy onset in stars around or below $\mathbf{0.7\,M_\odot}$, consistent with expectations, and the bending of tracks in stars around $\mathbf{1–3\,M_\odot}$ further indicates how internal physics evolve across the mass spectrum.

A comparison with **observational data** from **Gaia DR3** confirmed many features of the simulations. The main sequence constructed from Gaia data closely follows the slope and structure of the simulated HR tracks, particularly for solar-metallicity stars. However, some divergence is evident, such as a broader scatter of stars and the inclusion of post-main-sequence giants in the observational diagram. These differences are expected, given the greater diversity of real stars, including binary systems, rotation, mass loss, and varying metallicities not covered in the current model. It can also be inferred from the diagram that most of the star population lies between the mass tracks of $\mathbf{1\text{-}5M_\odot}$, while masses higher than $\mathbf{10M_\odot}$ are rare, which further strengthens our claim of instability of high mass stars according to the model.

Simulation-wise, the framework remained robust for most of the explored parameter space. However, as we pushed into more **extreme regimes** (particularly **high-mass, high-metallicity stars**) several limitations became apparent, both **physically and numerically**.

At Z = 0.04, simulations beyond $\mathbf{60M_\odot}$ frequently encountered failures. Some models ran to completion but produced no image outputs, while others terminated early. This instability is likely due to the combination of high radiation pressure and increased opacity in metal-rich stars, which creates internal configurations that are difficult to resolve without further physics such as enhanced mass loss or stricter timestep controls.

Above $\mathbf{\sim 80M_\odot}$, even stars at lower metallicities became problematic, especially during helium-burning phases. Many of these simulations encountered **"Out Of Memory" (OOM)** errors, primarily due to **timestep collapse**: as the models evolved, the necessary timestep became too small to process efficiently within available memory. Others reached the **maximum number of models (10,000)** without achieving the stopping condition.

Simulations with masses exceeding **100$M_\odot$** were especially fragile. Although some runs progressed partway, they often terminated prematurely or failed to meet the core hydrogen or helium depletion condition. The results for these stars have been included in the dataset for completeness, but they should be interpreted with caution, their evolutionary tracks are not reliable indicators of physical behavior.

Interestingly, a **"transition zone"** emerged between **60-80$M_\odot$**. In this range, convergence became inconsistent. Some stars evolved smoothly, while others failed midway through. The onset of instability appears to increase with both mass and metallicity, making this region particularly sensitive to simulation parameters.

The underlying causes of these terminations varied. A recurring issue involved MESA attempting to take a timestep smaller than the allowed minimum. In other cases, abrupt changes in energy generation or mesh resolution introduced instabilities that the solver couldn't handle.

All relevant simulation **logs**(`mesa.log`), **output files**, and **plots** have been preserved in the dataset hosted on **Zenodo**[2]. These records can serve as a reference for further debugging or future work aimed at extending these simulations more reliably into the very high-mass regime.

Overall, the simulation results affirm the predictive power of theoretical stellar models and highlight the value of computational tools like MESA. While certain physical effects and numerical limitations remain to be addressed, the trends captured in this project reflect real astrophysical behavior and offer a strong foundation for further extension and refinement.

Chapter 6
Conclusion

This project set out to model and visualize the evolution of stars using the MESA simulation code, exploring how variation in mass and metallicity impacts a star's lifecycle. By generating over 1200 simulations across six metallicity levels, this work provides a high resolution Stellar Evolution Atlas. Key stellar properties such as luminosity, temperature, radius and central composition were tracked to understand the evolutionary trends up to hydrogen and helium exhaustion.

The results successfully reproduced expected stellar behavior, including main-sequence tracks, degeneracy thresholds, and mass-luminosity relations, confirming the reliability of the theoretical models.The correlation between increasing mass and luminosity, as well as the impact of metallicity on temperature and opacity, aligned well with both theory and observational data from Gaia DR3.

Despite a strong foundation, challenges were encountered. Simulations at high masses **($\sim 80 M_\odot$)** and extreme metallicities (**$Z = 0.04$**) became unstable due to numerical or physical constraints. The results achieved highlights the strength and adaptability of MESA, and points to interesting regions of parameter space for future investigation.

I would like to express my sincere gratitude to the developers and maintainers of all the tools, libraries, and datasets that made this independent project possible. This work has made use of data from the European Space Agency (ESA) mission Gaia (https://www.cosmos.esa.int/gaia) , processed by the Gaia Data Processing and Analysis Consortium (DPAC, https://www.cosmos.esa.int/web/gaia/dpac/consortium). Funding for the DPAC has been provided by national institutions, in particular the institutions participating in the

Gaia Multilateral Agreement. I also acknowledge the creators of the MESA (Modules for Experiments in Stellar Astrophysics) software, which formed the backbone of the simulation engine in this project. Their efforts in developing and maintaining such a comprehensive tool are invaluable to the astrophysical community.

The plotting and data analysis in this project were carried out using Python libraries including `matplotlib`, `numpy`, `pandas`, and `astroquery`, and I thank their respective development communities for making them open-source and widely accessible.

I would also like to thank the creators of the `mesa_reader` library for simplifying the parsing and visualization of MESA outputs, and the developers of `ffmpeg` and `Streamlit` for enabling high-quality video and web deployment of simulation data.

Finally, I thank the authors of the references and books cited throughout the project, particularly Prialnik (2009), which served as the theoretical foundation for the study.

In the future, this Stellar Atlas could be extended to include advanced evolutionary stages, mass loss, rotation, and binary interactions. Further comparison with observational databases such as Gaia, SDSS, and LAMOST could help refine the physical models. We may also compare between different codes like Geneva stellar evolution code (https://www.unige.ch/sciences/astro/evolution/en/database) or PARSEC stellar tracks database (https://stev.oapd.inaf.it/PARSEC/). This project stands as a foundation for continued exploration of stellar astrophysics and computational modeling.

Chapter 7
References

[1] B. Paxton, L. Bildsten, A. Dotter, F. Herwig, P. Lesaffre, and F. Timmes, "Modules for Experiments in Stellar Astrophysics (MESA)," *The Astrophysical Journal Supplement Series*, vol. 192, p. 3, Jan. 2011, doi: 10.1088/0067-0049/192/1/3.

[2] A. Mishra, "Stellar Atlas Project: Simulation Dataset and Source Code." 2025. doi: <insert-doi-here>.

[3] D. Prialnik, *An Introduction to the Theory of Stellar Structure and Evolution*, 2nd ed. Cambridge: Cambridge University Press, 2009.

[4] B. Paxton *et al.*, "Modules for Experiments in Stellar Astrophysics (MESA): Planets, Oscillations, Rotation, and Massive Stars," *The Astrophysical Journal Supplement Series*, vol. 208, p. 4, Sep. 2013, doi: 10.1088/0067-0049/208/1/4.

[5] FFmpeg Team, "FFmpeg." [Online]. Available: https://ffmpeg.org/

[6] The Matplotlib Development Team, "Matplotlib: Visualization with Python (v3.10.3)." 2025. doi: 10.5281/zenodo.15375714.

[7] B. Wolf, "mesa-reader: Python library for parsing MESA output." [Online]. Available: https://github.com/wmwolf/mesa_reader

[8] M. Asplund, N. Grevesse, A. J. Sauval, and P. Scott, "The Chemical Composition of the Sun," *Annual Review of Astronomy and Astrophysics*, vol. 47, pp. 481–522, 2009, doi: 10.1146/annurev.astro.46.060407.145222.

[9] Streamlit Inc., "Streamlit: The fastest way to build data apps." [Online]. Available: https://streamlit.io/

[10] A. Mishra, "Stellar Atlas Project: Website Source Code." 2025.

[11] C. R. Harris *et al.*, "Array programming with NumPy," *Nature*, vol. 585, no. 7825, pp. 357–362, Sep. 2020, doi: 10.1038/s41586-020-2649-2.

[12] T. pandas development team, "pandas-dev/pandas: Pandas." [Online]. Available: https://doi.org/10.5281/zenodo.15597513

[13] A. Ginsburg *et al.*, “astroquery: An Astronomical Web-querying Package in Python,” *The Astronomical Journal*, vol. 157, no. 3, p. 98, Feb. 2019, doi: 10.3847/1538-3881/aafc33.

[14] Gaia Collaboration, T. Prusti, and others, “The Gaia mission,” *Astronomy & Astrophysics*, vol. 595, p. A1, 2016, doi: 10.1051/0004-6361/201629272.

[15] Gaia Collaboration, A. Brown, and others, “Gaia Data Release 3: Summary of the contents and survey properties,” *Astronomy & Astrophysics*, vol. 674, p. A1, 2023, doi: 10.1051/0004-6361/202243940.

Appendix A
Additional Material

In this section, we explore the **Zero-Age Main Sequence** (ZAMS) plots, which were not covered in earlier chapters due to focus on **post-ZAMS** evolution. These plots provide critical insight into the initial structure of stars at the onset of core hydrogen burning.

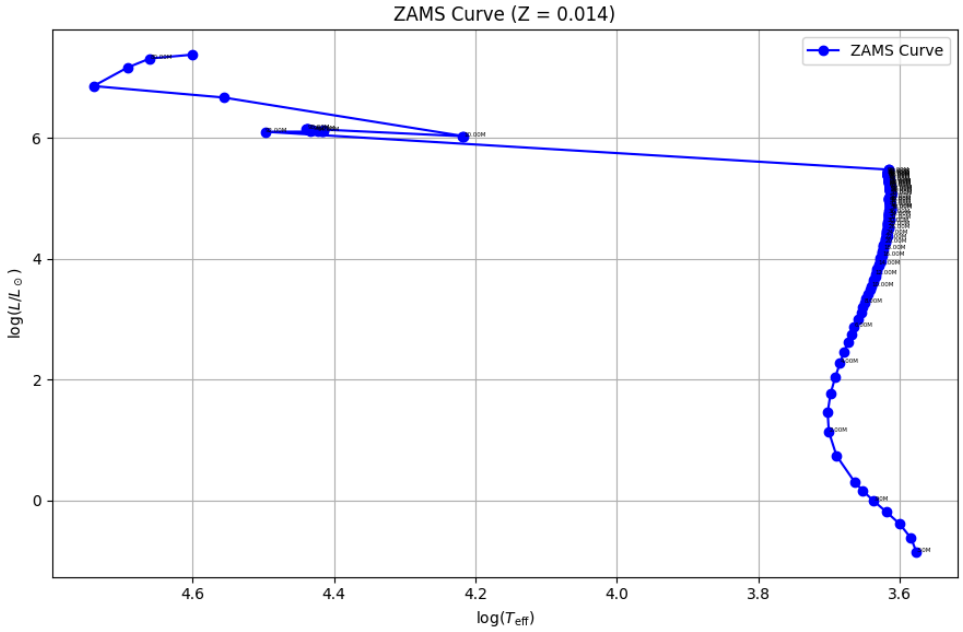

Figure A.17: Zero-Age Main Sequence (ZAMS) points for stars with **Z = 0.014**.

As expected, the initial luminosity increases with stellar mass, shifting the ZAMS points **upward and toward the left** on the HR diagram. This reflects the **higher surface temperatures** and **luminosities** of more massive stars. The transition is smooth for lower masses, but a sharp jump is observed near $\mathbf{90\,M_{\odot}}$, where the luminosity increases rapidly, consistent with theoretical mass-luminosity relations.

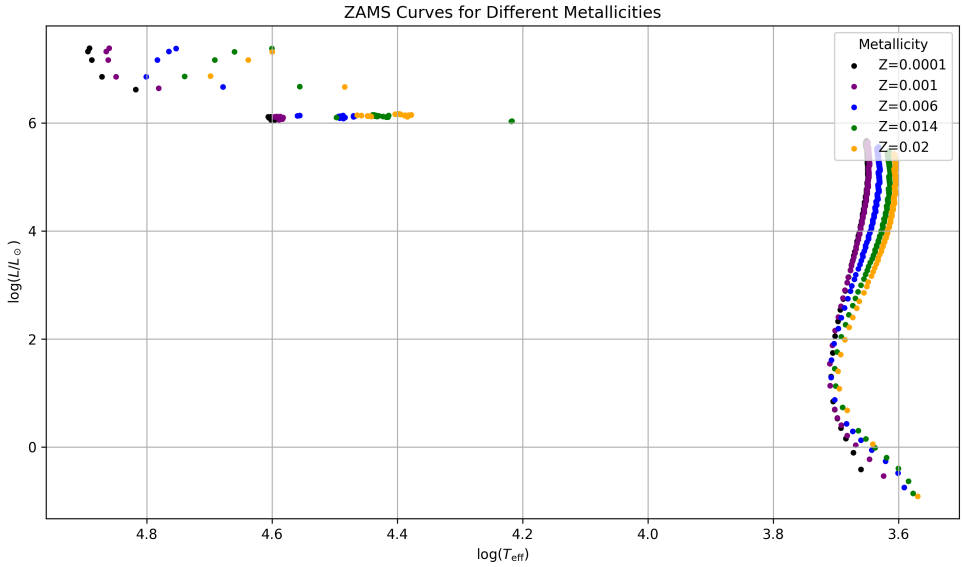

Figure A.18: Combined ZAMS HR diagram for all metallicities **except Z = 0.04** simulated in this study.

This expanded plot **(Figure A.18)** allows us to examine the impact of metallicity on stellar structure at birth. **As metallicity increases**:

- **ZAMS curves shift to the left**, indicating higher effective surface temperatures.
- For the same mass, **stars become slightly more luminous and less hot** with higher metallicity.
- These changes are attributed to **increased opacity**, which influences energy transport and thermal balance in stellar interiors.

This consolidated ZAMS view clearly demonstrates how both mass and metallicity influence a star's initial HR position before it begins significant evolution.

Appendix B
Codes and Simulation Data

This setup is **Linux compatible**. Since, I have windows on my system, I used **WSL (Windows Subsystem for Linux)** for the project. My system specs are as follows (Laptop - ACER PREDATOR HELIOS NEO 16 2023):

1. CPU: i7-13700HX
2. GPU: Nvidea RTX 4050 - 6GB Vram (**Even though the simulation is CPU intensive**)
3. RAM: 16GB

To run the Hydrogen Exhaustion simulations, it took around **12 hours** for a single metallicity, and for Helium Exhaustion, the time went up to around **20-24 hours**, sometimes even more than that.(Even though I could have just saved the hydrogen directly and continue the simulation from there, but I generated from the scratch to observe how much time it would take)

Due to the length and modular nature of the automation and analysis scripts used in this project, complete code listings are not printed in full here. However, the **complete codebase**, including bash scripts for simulation, Python scripts for post-processing and plotting, and configuration templates has been uploaded to **Zenodo**[2] and is publicly accessible alongside the dataset. Key portions of the code, along with explanations, are highlighted below for illustrative purposes.

Listing 2.1: The simulation roadmap

```
For each (mass, metallicity):
    --> Generate inlist from template
    --> Run MESA with customized config
    --> If success:
        --> Delete unnecassary files
        --> Plot outputs using rn.py
        --> Generate videos using ffmpeg
        --> Plot over all mass using plot_in_one.py
    --> Log any failures
```

The list of code files are as follows:

Listing 2.2: Code scripts list

```
1. Python script: Inlist_Gen.py
2. Bash script: run_batch_simulation.sh
    a. Python plotting script: rn.py
    b. Final plotting script: plot_in_one.py

The User only has to run the First and Second Script, the a and b
codes are run automatically due to the Bash Script.
```

The Simulation Directories are as follows:

1. **The Zenodo directory:**

```
Stellar_Atlas/
├── Hydrogen_Exhaustion/
│    ├── Z=0.0001_all_stars/
│    │       ├── 000.50M_0.0001Z_Stopping_Condn_h1_1d-5/
│    │       │       ├── LOGS/
│    │       │       │       └── history.data
│    │       │       ├── hr_evolution.mp4
│    │       │       ├── TRho_evolution.mp4
│    │       │       ├── hr_diagram.png
│    │       │       ├── age_vs_luminosity
│    │       │       ├── ... (more plots and videos)
│    │       │       └── metadata.json
│    │       ├── 001.00M_0.0001Z_Stopping_Condn_h1_1d-5\
│    │       └── ...\
│    ├── Z=0.001_all_stars/
│    │   ├── 000.50M_0.0001Z_Stopping_Condn_h1_1d-5/
│    │   └── ...\
└── Inlist_Gen/
     ├── mesa_inlists/
     ├── star_masses_summary.csv
     └── Inlist_Gen.py
└── README.md
```

Figure: Directory structure showing simulation outputs, metadata, and plots uploaded on Zenodo.

```
Stellar_Atlas/
├── Helium_Exhaustion/
│    ├── Z=0.0001_all_stars/
│    │       ├── 000.50M_0.0001Z_Stopping_Condn_h1_1d-5/
│    │       │       ├── LOGS/
│    │       │       │       └── history.data
│    │       │       ├── hr_evolution.mp4
│    │       │       ├── TRho_evolution.mp4
│    │       │       ├── hr_diagram.png
│    │       │       ├── age_vs_luminosity
│    │       │       ├── ... (more plots and videos)
│    │       │       └── metadata.json
│    │       ├── 001.00M_0.0001Z_Stopping_Condn_h1_1d-5\
│    │       └── ...\
│    └── Z=0.001_all_stars/
│        ├── 000.50M_0.0001Z_Stopping_Condn_h1_1d-5/
│        └── ...\
└── mesa_inlists/
     ├── Hydrogen_Exhaustion/
     │       ├── Z=0.0001/
     │       │   ├── inlist_000.50M_0.0001Z_...
     │       │   └── ... (all the inlists used)
     │       ├── Z=0.001/
     │       │      └── ...
     │       └── ...
     └── Helium_Exhaustion/
          ├── Z=0.0001/
          │   ├── inlist_000.50M_0.0001Z_...
          │   └── ... (all the inlists used)
          ├── Z=0.001/
          │      └── ...
          └── ...
```

Figure: Directory structure showing simulation outputs, metadata, and plots uploaded on Zenodo.

2. **The Website Directory (On Github):**

A Website was made to make the various graphs, plots, diagrams and videos available for dynamic use and proper comparison. Below is the directory structure of the website files. It is made using **streamlit**[9] and the files are available on **Github**[10]. The images and videos are embedded in the website directly from the source code directory.

Listing 2.3: Directory structure showing the Website hosted on streamlit, uploaded on Github

```
Stellar_Atlas/
        ├── .streamlit/
        │     └── Config.toml
        ├── assests/
        │     ├── Project_Report.pdf
        │     └── ...
        ├── pages/
        │     ├── 1_Atlas.py
        │     ├── 2_About_Me.py
        │     └── 3_Documentation.py
        ├── work/
        └── README.md
```

- **Simulation Scripts Summary:**

1. `Inlist_Gen.py` :

Listing 2.4: Inlist files generation

```
- Input: a csv file containing the initial mass,
metallicity, stopping condition and a short note.
- Output: The inlist files generated with the naming
convention: {mass}_{metallicity}_{stoppingcondition}
- Used in: Automating the generation of similar Inlist
files with limited changes using the same template
```

2. `rn.py` :
This Python script processes `history.data` files from MESA output and generates HR diagrams, temperature-density plots, age vs. luminosity, etc. The script uses the `mesa_reader` [7] library and `matplotlib` [6].

Listing 2.5: MESA output plotting script

```
- Input: path to `history.data`
- Output: PNG images
- Used in: automated post-processing after batch
simulations
```

3. `run_batch_simulations.sh` :
   This shell script runs the MESA simulation over all the inlist files (**210** at a time for a **single metallicity** from this project's perspective) in batch mode, handles directory creation, and invokes `rn.py` , `ffmpeg` and `plot_in_one.py` .

Listing 2.6: Bash Automation

```
- Input: The inlist files
- Output: MESA simulation, HR diagram and other plots,
ffmpeg videos, plots over all masses, pgstar plots.
- Used in: Automating the MESA simulation directory
generation, simulation running and binding together the
python codes to run automatically.
```

4. `plot_in_one.py` :

Listing 2.7: Generating plots over all masses

```
- Input: The history.data file across all masses for a
single metallicity.
- Output: The 210 simulations data plotted in a single plot
or diagram
- Used for: Generating comparitive plots to observe the
trends across simulations.
```

5. `GAIA_plot.py` :
   Used `Numpy` [11], `Pandas` [12] and `Astroquery` [13] in the code.

Listing 2.8: Plotting HR diagram using GAIA D3 dataset

```
- Input: history.data file across all masses for a given
metallicity and internet connection to proess the GAIA
query (ADQL query)
- Output: A plot with the MESA simulations data overlayed
with real life GAIA data
- Used for: Generating plots with both simulation data and
GAIA data.
```

6. `plot_all_ZAMS.py` :

   Listing 2.9: Generating the ZAMS plot in HR diagram across all stars in a single metallicity

```
- Input: All the history.data files across all the masses
for a single metallicity
- Output: A plot containing ZAMS of all the stars across
athe chosen metallicity
- Used for: Generating ZAMS plots.
```

7. `plot_all_ZAMS.py` :

   Listing 2.10: Generating the ZAMS plot in HR diagram across all metallicities for a given stopping condition

```
- Input: All the history.data files across all the masses
and all the metallicites for a given stopping condition
- Output: A plot containing ZAMS of all the stars across
all metallicities
- Used for: Generating ZAMS plots.
```

The In-depth and exact code files are available on Zenodo along with the dataset. The link for the same are:

1. **Zenodo Dataset[2]:**
2. **Project Website[10]:**
3. **MESA Website[1], [4]:** https://docs.mesastar.org/en/latest/index.html
4. **GAIA D3 Archive[14], [15]:** https://gea.esac.esa.int/archive/

Appendix C
Definitions

1. **Dynamical Stability:** refers to a system's ability to return to its original state after a disturbance
2. **Equation of state:** a mathematical relationship that describes how the pressure, volume, and temperature of a substance are related under specific conditions
3. **Opacity:** how well a material absorbs or scatters radiation
4. **Binding Energy:** Energy needed to break apart a system